



TECHNISCHE
UNIVERSITÄT
DARMSTADT

Institut für Kernphysik
Schloßgartenstraße 9
64289 Darmstadt, Germany

Bachelor-Thesis

BAG-MODEL STUDIES OF STRANGE AND
HYBRID STARS

UNTERSUCHUNG VON STRANGE STARS
UND HYBRIDSTERNEN IM BAG-MODELL

Pascal Büscher

Supervision: Professor Dr. Jochen Wambach
PD Dr. Michael Buballa

Date of Submission: 13.12.2006

Zusammenfassung

Durch numerische Integration der Tolman-Oppenheimer-Volkoff (TOV) Gleichung wird, unter Anwendung einer thermodynamischen Zustandsgleichung, die Struktur, d.h. eine Druck-Radius Funktion, und die Masse eines kompakten Sterns berechnet. In dieser Arbeit wird neben den Zustandsgleichungen idealer Fermi-Gase aus Neutronen bzw. Neutronen, Protonen und Elektronen, auch die des Bag-Modells angewandt. Dabei wird insbesondere darauf eingegangen, wie das Variieren der Bagkonstante und der Strange Quark Masse die für diese Parameter mögliche Maximalmasse der Strange Stars beeinflusst. Auf die Diskussion der Strange Stars folgt eine kurze Betrachtung von Hybridsternen.

Abstract

By integrating the Tolman-Oppenheimer-Volkoff (TOV) equation numerically and by applying an equation of state (EoS), the structure, i.e. the pressure as a function of the radius, and the mass of a compact star are computed. Beside the EoS of ideal Fermi gases consisting of neutrons or neutrons, protons, and electrons, the EoS of the bag model is employed in this work. Moreover, it is investigated how varying the bag constant and the strange quark mass affects the mass limit of strange stars. After the discussion of strange stars, hybrid stars are briefly discussed.

Contents

1	Introduction	2
2	The Underlying Theory	3
2.0.1	Units	3
2.0.2	Zero Temperature	3
2.1	General Relativity and the Tolman-Oppenheimer-Volkoff Equation . .	3
2.1.1	Expressions from General Relativity	3
2.1.2	The Schwarzschild Solution	5
2.1.3	The Tolman-Oppenheimer-Volkoff Equation	5
2.1.4	The TOV Equation as an Equation of the Chemical Potential μ	6
2.2	The Equation of State for a Cold Degenerate Ideal Fermi Gas	7
3	Computational Details	9
3.1	Constants	9
3.2	Integration	9
3.3	The Break Condition	10
3.4	The Iteration for Finding the Mass Limit	10
4	Pure Neutron Stars	11
4.1	A Star's Structure	11
4.2	$M(R)$ and the Mass Limit	11
5	Compact Stars of Neutrons, Protons and Electrons	13
5.1	The Equation of State	14
5.2	Charge Neutrality	15
5.3	Results	15
6	Strange Stars	17
6.1	The Equation of State	17
6.2	Charge Neutrality	19
6.3	Results	20
6.3.1	The Influence of the Bag Constant B	20
6.3.2	The Influence of the Strange Quark Mass m_s	25
7	Hybrid Stars	28
7.1	The Hadronic Phase	28
7.2	The Phase Transition	28
7.3	Results	29
8	Summary and Outlook	32

1 Introduction

In 1939, Tolman [1] and Oppenheimer and Volkoff [2] were the first to solve the Einstein field equations for stars that are relativistic, static, and spherically symmetric. By adopting their result, the Tolman-Oppenheimer-Volkoff equation, and by employing an equation of state (EoS), it is possible to (numerically) compute the pressure inside a compact star as a function of its radius. With the EoS other quantities like the energy density and number density can be obtained.

Moreover, knowing the pressure in terms of the radius enables us to find the star's radius and even its mass. Inside the star the pressure has to be positive to support matter against being torn towards the center. However, at the surface, the pressure has to be 0, because the star would otherwise expand. By applying this condition, the radius can be obtained from the solution of the Tolman-Oppenheimer-Volkoff equation. Consequently, the mass is a by-product of the above calculations. If one carries out these calculations for several parameters, one finds that there is a maximum of the mass.

This mass limit (as well as a star's structure) strongly depends on the applied EoS. Although four different EoS are applied in this work, the emphasis is on the bag model. The model is similar to an ideal, degenerate Fermi gas of quarks, whereas pressure and energy density are shifted by the bag constant B . The bag constant represents confinement, an effect preventing quarks from being isolated. This work aims to investigate the influence of B and of the strange quark mass m_s on compact stars computed with the EoS of the bag model. The strange quark mass is of interest, because quark masses cannot be determined like the mass of e.g. electrons. The strange quark mass is chosen, since it is by far the heaviest compared to the other quark masses. Hence, the effects are expected to be strongest for strange quarks.

This work starts by giving a succinct derivation of the Tolman-Oppenheimer-Volkoff equation (section 2.1), some information on the equation of state for cold Fermi gases (section 2.2) and details on how the computing was accomplished (section 3).

After this, there are four sections, each tackling the Tolman-Oppenheimer-Volkoff equation for another equation of state. The first two EoS handle cold ideal and degenerate Fermi gases: the first one (section 4) consisting only of neutrons and the second one consisting of neutrons, protons and electrons (section 5). In section 6, the above mentioned bag model will be dealt with. In section 7, hybrid stars, i.e. stars consisting of a quark and a hadronic phase, will be briefly discussed. While the first two EoS were mainly calculated for testing reasons and while the hybrid star section was included as an add-on, this work's emphasis is on the bag model.

2 The Underlying Theory

2.0.1 Units

Throughout this work, units were chosen that $c = \hbar = 1$ for convenience. When employing constants and parameters, units have to be converted to this system by multiplying the right combination of c and \hbar . Length units are, for example, converted into reciprocal energy units by multiplying $(\hbar c)^{-1}$. More information on units and their conversion may be found in chapter 3.3 of [3].

2.0.2 Zero Temperature

Although the temperature in compact stars cannot be considered cold on any earthy scale, the effect of temperature can be neglected when calculating pressure and energy. Shortly after neutron stars are born, they have temperatures of about 10^{10} K. Within 1 million years, a neutron star's temperature decreases to 10^6 K [3]. This temperature corresponds to about 0.1 keV, which is small compared to the energies of several hundred MeV that we will encounter in the following sections.

2.1 General Relativity and the Tolman-Oppenheimer-Volkoff Equation

To fully understand where the Tolman-Oppenheimer-Volkoff (TOV) equations originate, it is crucial to understand general relativity. If necessary, the reader may consult [4] or any other book on General Relativity.

2.1.1 Expressions from General Relativity

At first, we want to recapitulate some definitions and relations of general relativity. All relations shown here are taken from [3] to avoid confusion in respect of notations. In general relativity, the metric tensor $g_{\mu\nu}$ has the same function that the Minkowski tensor $\eta_{\mu\nu}$ has in special relativity. In contrast to the Minkowski tensor, $g_{\mu\nu}$ is a function of space and time. $g_{\mu\nu}$ can be employed to transform any contravariant four quantity into its covariant counterpart (one says that an index is "lowered"). For the converse transformation (for "raising" an index) one defines the inverse of $g_{\mu\nu}$, that is $g^{\mu\nu}$.

The affine connection $\Gamma_{\mu\nu}^\lambda$ can be defined as

$$\Gamma_{\mu\nu}^\lambda \equiv \frac{\partial x^\lambda}{\partial \xi^\alpha} \frac{\partial^2 \xi^\alpha}{\partial x^\mu \partial x^\nu} \quad (2.1)$$

where ξ^α are the coordinates of a freely falling, locally inertial frame. x^μ are the coordinates of the chosen frame. The motivation for this definition is that the equation of motion of a freely falling particle is determined by $\frac{d^2 x^\lambda}{d\tau^2} + \Gamma_{\mu\nu}^\lambda \frac{dx^\mu}{d\tau} \frac{dx^\nu}{d\tau} = 0$. The path of such a particle, which is described by the line element $d\tau$ ($d\tau$ will be introduced for spherical coordinates in (2.12)), is called a geodesic.

We may also express the affine connection $\Gamma_{\mu\nu}^\lambda$ in terms of the metric tensor

$$\Gamma_{\mu\nu}^\lambda = \frac{1}{2} g^{\lambda\kappa} (g_{\kappa\nu,\mu} + g_{\kappa\mu,\nu} - g_{\mu\nu,\kappa}) \quad (2.2)$$

where the comma subscript notation (e.g. $_{,\mu}$) represents the coordinate derivative, i.e. for example $g_{\kappa\nu,\mu} = \frac{d}{dx^\mu} g_{\kappa\nu}$.

The definition of covariant divergence for an arbitrary contravariant/covariant vector is given by

$$A^\mu_{;\nu} \equiv A^\mu_{,\nu} + \Gamma^\mu_{\sigma\nu} A^\sigma \quad A_{\mu;\nu} \equiv A_{\mu,\nu} + \Gamma^\lambda_{\mu\nu} A_\lambda \quad (2.3)$$

The Riemann(-Christoffel curvature) tensor $R^\rho_{\sigma\mu\nu}$ is defined as

$$R^\rho_{\sigma\mu\nu} \equiv \Gamma^\rho_{\sigma\nu,\mu} - \Gamma^\rho_{\sigma\mu,\nu} + \Gamma^\alpha_{\sigma\nu} \Gamma^\rho_{\alpha\mu} - \Gamma^\alpha_{\sigma\mu} \Gamma^\rho_{\alpha\nu} \quad (2.4)$$

From the Riemann tensor we obtain the Ricci tensor

$$R_{\mu\nu} = R^\rho_{\mu\nu\rho} \quad (2.5)$$

Using the definition of the Riemann tensor (2.4), we rewrite the Ricci tensor as

$$R_{\mu\nu} = \Gamma^\alpha_{\mu\alpha,\nu} - \Gamma^\alpha_{\mu\nu,\alpha} - \Gamma^\alpha_{\mu\nu} \Gamma^\beta_{\alpha\beta} + \Gamma^\alpha_{\mu\beta} \Gamma^\beta_{\nu\alpha} \quad (2.6)$$

We now define the scalar curvature R

$$R = g^{\mu\nu} R_{\mu\nu} \quad (2.7)$$

By applying (2.3) multiple times, one may acquire the third covariant derivative of an arbitrary covariant vector, and use the result to obtain the Bianchi identity

$$R^\alpha_{\mu\nu\rho;\sigma} + R^\alpha_{\mu\sigma\nu;\rho} + R^\alpha_{\mu\rho\sigma;\nu} = 0 \quad (2.8)$$

The Bianchi identity (2.8) can now be multiplied by $g^{\mu\nu}$ and transformed, so that we arrive at

$$(R^{\mu\nu} - \frac{1}{2}g^{\mu\nu}R)_{;\nu} = 0 \quad (2.9)$$

From the above equation, one may derive the Einstein field equations

$$R^{\mu\nu} - \frac{1}{2}g^{\mu\nu}R \equiv G^{\mu\nu} = -8\pi GT^{\mu\nu} \quad (2.10)$$

where $G^{\mu\nu}$ is the Einstein curvature tensor. $T^{\mu\nu}$ denotes the energy-momentum tensor. For a static star the energy-momentum tensor is given by

$$T_0^0 = \epsilon, \quad T_\mu^\mu = -p, \quad (\mu \neq 0); \quad T_\mu^\nu = 0 \text{ for } \mu \neq \nu \quad (2.11)$$

with the pressure p and the energy density ϵ . We apply the relations found above to a spherical star. There, it is advisable to use spherical coordinates. The line element can then be expressed as

$$d\tau^2 = e^{2\nu(r)} dt^2 - e^{2\lambda(r)} dr^2 - r^2 d\theta^2 - r^2 \sin^2\theta d\phi^2 \quad (2.12)$$

Comparison with $d\tau^2 = g_{\mu\nu} dx^\mu dx^\nu$ shows that

$$g_{00} = e^{2\nu(r)}, \quad g_{11} = -e^{2\lambda(r)}, \quad g_{22} = -r^2, \quad g_{33} = -r^2 \sin^2\theta; \quad g_{\mu\nu} = 0 \text{ for } \mu \neq \nu \quad (2.13)$$

For this metric, we find the following components of the Ricci tensor

$$\begin{aligned}
R_{00} &= \left(-\nu'' + \lambda'\nu' - \nu'^2 - \frac{2\nu'}{r} \right) e^{2(\nu-\lambda)} \\
R_{11} &= \nu'' - \lambda'\nu' + \nu'^2 - \frac{2\lambda'}{r} \\
R_{22} &= (1 + r\nu' - r\lambda')e^{-2\lambda} - 1 \\
R_{33} &= R_{22} \sin^2 \theta
\end{aligned} \tag{2.14}$$

The primes denote differentiation with respect to r .

2.1.2 The Schwarzschild Solution

In the empty space outside a star, pressure and energy density have to vanish. We may thus formulate the field equations as

$$R^{\mu\nu} - \frac{1}{2}g^{\mu\nu}R \equiv G^{\mu\nu} = 0 \tag{2.15}$$

With the definition of R (2.7), it can be shown that $R = 0$. Applying (2.14), one determines $e^{\nu(r)}$ and $e^{\lambda(r)}$. Employing these two functions in (2.13), one finds the Schwarzschild solution:

$$\begin{aligned}
g_{00} &= e^{2\nu(r)} = \left(1 - \frac{2GM}{r} \right) \\
g_{11} &= -e^{2\lambda(r)} = - \left(1 - \frac{2GM}{r} \right)^{-1} \\
g_{22} &= -r^2, \quad g_{33} = -r^2 \sin^2 \theta; \quad g_{\mu\nu} = 0 \text{ for } \mu \neq \nu \text{ (as in (2.13))}
\end{aligned} \tag{2.16}$$

M and G were introduced as constants of integration. G corresponds to Newton's Gravitational constant. M denotes the star's mass.

2.1.3 The Tolman-Oppenheimer-Volkoff Equation

Inside a spherical star, pressure and energy density are not vanishing quantities. Employing (2.14) in (2.10), we obtain the function $e^{-2\lambda(r)}$, which now depends on ϵ .

$$e^{-2\lambda(r)} = 1 - \frac{8\pi G}{r} \int_0^r \epsilon(r') r'^2 dr' \tag{2.17}$$

At the surface, the same results have to be returned by the Tolman-Oppenheimer-Volkoff solution and the Schwarzschild solution. Comparing (2.17) with (2.16), we may define

$$M(r) = 4\pi \int_0^r r'^2 \epsilon dr' \tag{2.18}$$

$M(r)$ gives the mass included in a sphere with the same center as the neutron star and the radius r . With this definition, we find $M_{Schwarzschild} = M_{TOV}(R)^1$ (with R being the star's radius).

¹In this equation the masses defined in the two solutions have been labeled with indices for clarity

We apply (2.14) to the Einstein field equations to obtain λ' , ν' , ν'' , and ν'^2 in terms of p , p' , and ϵ . With these relations, p' can be expressed in terms of p and ϵ . We emerge with the Tolman-Oppenheimer-Volkoff (TOV) equation.

$$\frac{dp(r)}{dr} = -\frac{G(p(r) + \epsilon(r))(M(r) + 4\pi r^3 p(r))}{r(r - 2GM(r))} \quad (2.19)$$

2.1.4 The TOV Equation as an Equation of the Chemical Potential μ

For most thermodynamic models, it is much easier to obtain ϵ and p in terms of the chemical potential μ instead of obtaining ϵ in terms of p . Therefore, a modified version of the TOV equation is derived in this subsection. As discussed in this section, the modification applies only to models consisting of only one chemical potential, i.e. only of one kind of particle. We will extend the modification to models that have multiple chemical potentials in section 5. As for now, the pressure can be expressed as a function of only the chemical potential, which is defined as the energy needed to add a particle to the system. We may then write the left hand side of the TOV equation as

$$\frac{dp}{dr} = \frac{dp}{d\mu} \frac{d\mu}{dr} \quad (2.20)$$

From the Gibbs-Duhem relation

$$0 = S dT - V dp + \sum_i N_i d\mu_i \quad (2.21)$$

it can be seen that, under the prerequisites that $dT = 0$ ² and that we have only one chemical potential, $\frac{dp}{d\mu}$ is given by:

$$\frac{dp}{d\mu} = \frac{N}{V} = \rho \quad (2.22)$$

where ρ is the particle density. The pressure p is defined as

$$p = -\frac{\partial E}{\partial V} \quad (2.23)$$

The equation has still to be valid, if E and V are interpreted as the energy per particle and volume per particle. With this interpretation, p can be written as

$$p = -\frac{\partial \left(\frac{E}{N}\right)}{\partial \left(\frac{V}{N}\right)} = -\frac{\partial}{\partial \frac{1}{\rho}} \left(\frac{\epsilon}{\rho}\right) = \rho^2 \frac{\partial}{\partial \rho} \left(\frac{\epsilon}{\rho}\right) = \rho\mu - \epsilon \quad (2.24)$$

where $\mu \equiv \frac{d\epsilon}{d\rho}$ was used. The above equations can also be found in [3].

With (2.20), (2.22), and (2.24), the TOV equation (2.19) can be written as

$$\frac{d\mu}{dr} = -\frac{G\mu(M + 4\pi r^3 p)}{r(r - 2GM)} \quad (2.25)$$

²This is a consequence of our approximation that $T = 0$. We implied that $T = 0$ everywhere in the star, which leads to $dT = 0$.

2.2 The Equation of State for a Cold Degenerate Ideal Fermi Gas

For an ideal cold quantum gas, the momentum of a particle in a cube with the side length L is given by [5]

$$\vec{k}_n = \frac{2\pi\hbar}{L}\vec{n} = \frac{2\pi}{L}\vec{n} \quad (2.26)$$

with the components of \vec{n} (n_x , n_y , and n_z) denoting the states of the three spatial coordinates x , y , and z . In the second step, we have applied that $\hbar = 1$ in our units.

Since we have made the assumption that the particles do not interact, we expect to find a particle of a state in a volume, independently of the existence of particles of different states within the same volume. Hence, summing over all states will give us the total particle density. In the limit of a continuum ($V \rightarrow \infty$), there is an infinite number of states. Instead of computing a sum, we now have to carry out an integration. We write

$$\rho = \frac{N}{V} = \frac{\int_0^\infty d^3n f(\vec{n})}{V} \quad (2.27)$$

$f(\vec{n})$ is the distribution function, which gives the particle density for every state. Substituting n with k for all dimensions yields

$$\rho = \frac{1}{V} \int_0^\infty d^3k f(\vec{k}) \left(\frac{\partial n_x}{\partial k_x} \right) \left(\frac{\partial n_y}{\partial k_y} \right) \left(\frac{\partial n_z}{\partial k_z} \right) \quad (2.28)$$

The derivatives can be obtained from (2.26). We have

$$\frac{\partial n_i}{\partial k_i} = \frac{L}{2\pi} \quad \text{for } i = x, y, z \quad (2.29)$$

From the assumption of $T = 0$ (see sec. 2.0.2) and the Pauli exclusion principle, we know that all states with energies below the chemical potential μ are completely filled. The particle distribution function in terms of the particle's momentum k may now be written as $f(\vec{k}) = 2\Theta(k_F - k)$, where Θ denotes the step function and k_F the Fermi momentum (the maximum momentum allowed for a given μ). The factor of 2 originates from the two spin options neutrons (as well as protons and electrons) have. Consequently, we may write ρ as

$$\rho = \int_0^\infty \frac{d^3k}{(2\pi)^3} \frac{L^3}{V} 2\Theta(k_F - k) = \int_0^{k_F} \frac{8\pi k^2 dk}{(2\pi)^3} \quad (2.30)$$

In the last step, we used the isotropy of space, which allows us to integrate in spherical coordinates. We carry out the integration to obtain

$$\rho = \frac{k_F^3}{3\pi^2} \quad (2.31)$$

In order to obtain the energy density ϵ , we have to multiply the integrand of (2.30) with the energy per state ϵ_i . This energy can be expressed as

$$\epsilon_i = \sqrt{k^2 + m^2} \quad (2.32)$$

Analogously to (2.30), we find

$$\epsilon = \int_0^{k_F} dk \frac{8\pi}{(2\pi)^3} k^2 \sqrt{k^2 + m^2} \quad (2.33)$$

This integral can be looked up in tables like the one in [6].

$$\epsilon = \frac{1}{\pi^2} \left(\frac{k_F}{4} (k_F^2 + m^2)^{3/2} - \frac{m^2}{8} \left(k_F \sqrt{k_F^2 + m^2} + m^2 \ln \left(\frac{k_F + \sqrt{k_F^2 + m^2}}{m} \right) \right) \right) \quad (2.34)$$

Using that with (2.32) μ can be identified as

$$\mu = \sqrt{k_F^2 + m^2} \quad (2.35)$$

we arrive at

$$\epsilon = \frac{1}{8\pi^2} \left(\mu k_F (2\mu^2 - m^2) - m^4 \ln \left(\frac{k_F + \mu}{m} \right) \right) \quad (2.36)$$

Having derived ρ and ϵ , the pressure can be obtained by applying (2.24).

$$\begin{aligned} p &= -\frac{1}{8\pi^2} \left(\mu k_F (2\mu^2 - m^2) - m^4 \ln \left(\frac{k_F + \mu}{m} \right) \right) + \mu \frac{k_F^3}{3\pi^2} \\ &= \frac{1}{24\pi^2} \left(\mu k_F (2\mu^2 - 5m^2) + 3m^4 \ln \left(\frac{k_F + \mu}{m} \right) \right) \end{aligned} \quad (2.37)$$

3 Calculational Details

3.1 Constants

Except for the quark masses, all necessary constants were taken from the GSL [7]. The GSL constants are mostly identical to the constants of the Review of Particle Physics [8] within the uncertainty given in [8]. Only the solar mass M_{\odot} and gravitational constant G were found to be slightly smaller in the GSL libraries. The up and down quark masses in section 6 were taken from [3]. The strange quark mass was taken as a parameter and will be varied in the strange star section.

3.2 Integration

The actual calculation of a star's structure is done by integrating from the star's center to its surface. Starting at the center, we need a given initial value for p or μ and have to choose a stepwidth. The stepwidth should be small enough, so that we can assume that μ , p , ϵ , and M are constant within a step.

All calculations in this work were performed with the modified equation (2.25). Nevertheless, most steps in this section could be done for calculations with (2.19) in an analogous manner. For every step, the change of μ and M is calculated with

$$\Delta\mu = -\frac{G\mu(M + 4\pi r^3 p)}{r(r - 2GM)}\Delta r \quad (3.1)$$

$$\Delta M = 4\pi r^2 \epsilon \Delta r \quad (3.2)$$

(3.2) is based on the idea that with every step, a thin layer is added to the sphere for which the mass is calculated. This approximation works well for large radii. As for the first few steps (r is of the same magnitude as the stepwidth) the layer is not thin compared to the sphere. For this area, a formula that gives better results should be used. With (2.18) and the assumption that ϵ is constant within a step, we find that

$$\Delta M = \int_r^{r+\Delta r} 4\pi r'^2 \epsilon dr' = 4\pi\epsilon \left(r^2\Delta r + r(\Delta r)^2 + \frac{1}{3}(\Delta r)^3 \right) \quad (3.3)$$

For large r (3.3) is still valid; however, since $\Delta r \ll r$, (3.2) is a good approximation that slightly accelerates calculations. For the first step, we have to cope with another problem. The denominator of (2.25) vanishes for $r = 0$. However, by applying that $M(r) = \epsilon \int_0^r 4\pi r'^2 dr' = \frac{4}{3}\pi r^3 \epsilon$ for small r , (3.1) yields

$$\Delta\mu = \lim_{r \rightarrow 0} \left(-\frac{G\mu(\frac{4}{3}\pi r^3 \epsilon + 4\pi r^3 p)}{r(r - \frac{8}{3}G\pi r^3 \epsilon)} \right) \Delta r = 0 \quad (3.4)$$

By comparing different modifications for small radii (like (3.3)), it was found that their effect is negligible. For the pure neutron model (See sec. 4) the maximum effect on the star's mass was below 0.0003%, the effect on the radius was of similar magnitude.

3.3 The Break Condition

With the above expressions, the integration can be conducted from the center to the surface R . We know that the surface is reached, when we find that $p = 0$ (In the numerical integration the actual condition is $p < 0$). Inside the star, the pressure has to be positive to support matter against falling towards the center. At a point where $p = 0$, there is no pressure that could prevent that matter is torn towards the center by gravitation [3]. This point must thus lie on the surface.

At the surface, the solution of Schwarzschild has to hold true, as well as the solution of Tolman, Oppenheimer, and Volkoff. Therefore, all elements of the energy-momentum tensor $T^{\mu\nu}$ have to vanish at the surface. This means that $p(R) = 0$ and $\epsilon(R) = 0$. From the above argumentation it is clear that p has to be continuous even at the surface. In section 6, one will see that this does not necessarily hold true for ϵ .

3.4 The Iteration for Finding the Mass Limit

In the following sections, the maximum mass plays an important role. The rather simple algorithm for finding those maxima is thus briefly discussed here. At first, the program calculates a star's mass for a given initial value of the chemical potential. After that, the initial chemical potential is raised by a stepwidth j , and the mass is calculated again for the new parameter. For each step, the program checks, if the new value of the mass exceeds the last one. If it does, the program proceeds, adding j to the initial chemical potential. If not, the program has to further investigate the last two sections. j is then changed to $j_{new} = -j/2$. The maximum is then approached from the other direction with a smaller stepwidth. This procedure is repeated until a certain number of configurations have been computed (depending on the calculation 30 or 35 stars). Since the maximum is approached from both directions with this method, we may interpret the variation in the last few steps as an indicator for the precision of our iteration procedure. The method was found to converge with no changes occurring on at least the first six significant digits during these last steps.

Note that this method is limited to continuous functions with only one maximum. Continuity is fulfilled, since all EoS treated in this work are continuous. The condition of only one maximum is not fulfilled for all values of the initial chemical potential. In the unstable region of high pressure (see the end of the next section), we can find some more maxima. We work around this problem here, by approaching the maximum from low initial values. Only if the program exceeds the first minimum after the maximum, it is likely to converge to the wrong maximum. Since much higher pressures are needed to receive results in that region, one can assume that the program will converge to the right maximum for any reasonable choice of the initial values. One could of course argue that the method described here is heading only for the first maximum, which is not necessarily the global maximum. Although it is not proven in this work that there is no maximum higher than the first one, there was no function giving a hint that it would rise to the level of the first maximum again at some other point.

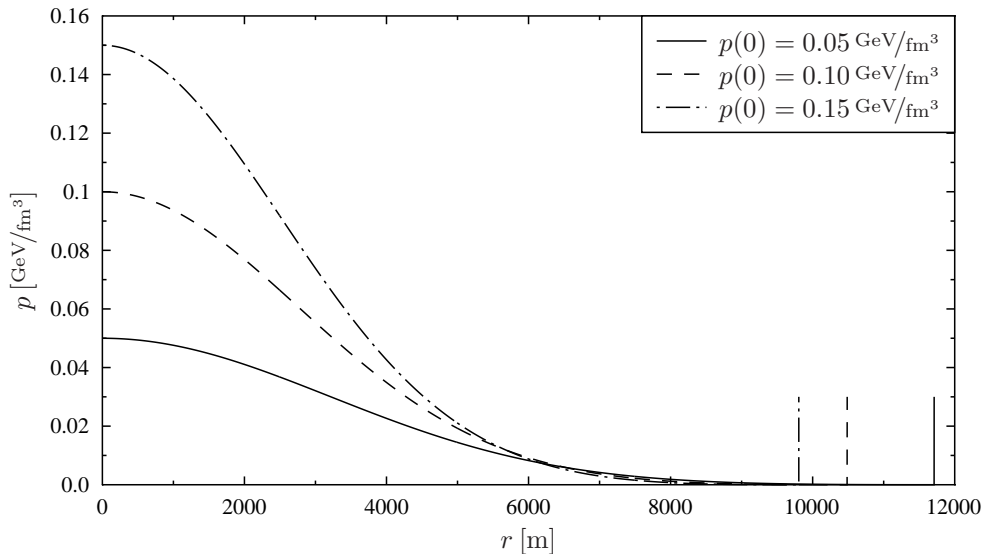


Figure 1: The pressure p inside a pure neutron star plotted over the distance r from the center for different values of the central pressure $p(0)$. The vertical lines at the right mark the stars' surfaces R .

4 Pure Neutron Stars

The simplest model for a neutron star is one consisting of a Fermi gas of non-interacting neutrons. In this model, we can directly employ the expressions for the equation of state derived in section 2.2, where the constant m is the neutron mass. By applying the calculation procedure described in section 3, this section's results were obtained.

4.1 A Star's Structure

In order to compare the results with other calculations that used the "original" Oppenheimer-Volkoff equation (2.19), p was plotted as a function of r in figure 1. By employing the EoS, other quantities like the number density or energy density could be expressed in terms of the radius. We may therefore say that a star's structure is known, when $p(r)$ is known. The obtained results were found to be in very good accordance with the results of other calculations [9].

4.2 $M(R)$ and the Mass Limit

If one carries out the above calculations for various initial values of μ , the stars' mass M can be plotted over the stars' radii R .

In figure 2, we find that there is a maximum mass. Although it may sound surprising at first, the explanation of the occurrence of a mass limit is simple. Stars of high mass have to have high pressure at the center, because all mass is attracted to the center by gravitation [3]. In (2.25) one finds μ on the right side of the TOV equation. The

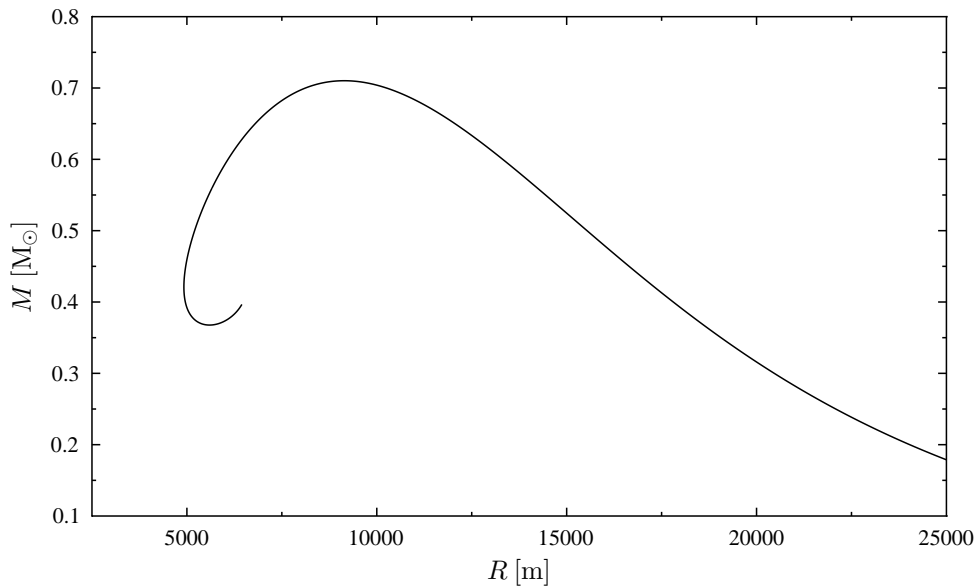


Figure 2: This plot depicts the mass over the radius for different values of the initial chemical potential. The maximum of the mass is $0.7102 M_{\odot}$ (M_{\odot} being the solar mass) at 9142 m. Low initial pressures have big radii, high initial pressures small radii.

energy density and the pressure are both strictly monotonic functions of μ as (2.37) and (2.36) reveal. With this in mind, we may conclude that for a large pressure, i.e. a large chemical potential μ , the derivative will be even larger. The star's surface will then be reached at a small radius. However, for a small radius, there will not be much mass included in the star. If a star exceeds the mass limit, it will collapse to a black hole [3]. The phenomenon of a limiting mass is not limited to this model. In fact, it is shown in [3] that with only a few basic assumptions, such a maximum mass will be encountered in any model. The pure neutron model has a rather small limiting mass. In a model including nucleon interaction the limiting mass would be found to be higher, since repulsive forces would increase the pressure and thus support the star against collapse [3].

For all solutions to the left of the maximum in figure 2 (stars with a higher initial pressure), the star's mass is decreased for an increased pressure, according to our calculations. However, if mass is added to a star, the pressure at the center has to be increased due to the gravitational attraction of the mass. This contradiction shows that these solutions of the TOV equation must be unstable.

5 Compact Stars of Neutrons, Protons and Electrons

The model we employed in section 4 is as simple as unrealistic. One of the phenomena that we have totally neglected so far is neutron decay. Free neutrons have a mean lifetime of about 15 minutes [8]. Their decay is given by

$$n \rightarrow p + e^- + \bar{\nu}_e \quad (5.1)$$

Due to beta decay, we expect that there will be electrons and protons besides the neutrons. However, if there are protons and electrons in the star, we will also encounter electron capture reactions - the inverse process of (5.1). The antineutrinos $\bar{\nu}_e$ and the neutrinos ν_e that evolve from the decay reactions are able to escape the star due to their extremely small cross section with nucleons and electrons. Having in mind that we are handling a cold Fermi gas, we can conclude from the Pauli exclusion principle that the equilibrium state of these two reactions will be achieved, when

$$\mu_n = \mu_p + \mu_e \quad (5.2)$$

As a consequence, we now have only two independent chemical potentials. We choose to write

$$\begin{aligned} \mu_n &= \mu_B \\ \mu_p &= \mu_B + \mu_Q \\ \mu_e &= -\mu_Q \end{aligned} \quad (5.3)$$

where μ_B denotes the baryon potential and μ_Q the chemical potential of charge. The factors in front of μ_Q and μ_B represent electric charge (in e) and the baryon number of the corresponding particle. Both, electric charge and baryon number, are conserved under all other processes observed in physics. Due to their negative charge, μ_Q has to be negative for electrons to exist.

In section 2.1.4, we have shown that we can modify the TOV to obtain a differential equation in terms of μ instead of p . We still have to show that there is a modified TOV for two chemical potentials under the condition of charge neutrality (see section 5.2 for the discussion of charge neutrality) and baryon number conservation. Employing the Gibbs-Duhem relation

$$0 = S dT - V dp + \sum_i N_i d\mu_i \quad (5.4)$$

we find for $T = dT = 0$

$$dp = \sum_i \frac{N_i}{V} d\mu_i = \sum_i \rho_i d\mu_i \quad (5.5)$$

Due to charge neutrality, we may express all chemical potentials as functions of one chemical potential μ_k . Hence, we may write

$$dp = \left(\sum_i \rho_i \frac{d\mu_i}{d\mu_k} \right) d\mu_k \quad (5.6)$$

Since we have chosen μ_Q as a chemical potential, we may express charge neutrality as $\rho_Q = 0$. With μ_B as the other chemical potential, the above equation is then reduced to

$$dp = \rho_B d\mu_B \quad (5.7)$$

The relation (2.24) connecting p and ϵ for the case of one chemical potential can be extended to the case of more than one chemical potential. There, we find

$$p = \sum_i \rho_i \mu_i - \epsilon \quad (5.8)$$

Applying charge neutrality, i.e. $\rho_Q = 0$, again, the above equation yields

$$p = \rho_B \mu_B - \epsilon \quad (5.9)$$

We can now rewrite the TOV as

$$\frac{d\mu_B}{dr} = -\frac{G\mu_B(M + 4\pi r^3 p)}{r(r - 2GM)} \quad (5.10)$$

5.1 The Equation of State

With the conditions of section 2.2 (especially the disregard of any particle-particle interaction), we obtain the same number densities as in (2.31) for each kind of particle.

$$\rho_n = \frac{k_n^3}{3\pi^2}, \quad \rho_p = \frac{k_p^3}{3\pi^2}, \quad \rho_e = \frac{k_e^3}{3\pi^2} \quad (5.11)$$

where k_n , k_p , and k_e are the Fermi momenta of neutrons, protons, and electrons respectively³. These Fermi momenta can be expressed analogously to (2.35).

For each kind of particle, we deduce the energy density as described in section 2.2. These particle energy densities are then added up to

$$\begin{aligned} \epsilon &= \sum_{i=e,n,p} \epsilon_i \\ &= \frac{1}{8\pi^2} \left(\mu_B k_n (2\mu_B^2 - m_n^2) - m_n^4 \ln \left(\frac{k_n + \mu_B}{m_n} \right) \right. \\ &\quad + (\mu_B + \mu_Q) k_p (2(\mu_B + \mu_Q)^2 - m_p^2) - m_p^4 \ln \left(\frac{k_p + \mu_B + \mu_Q}{m_p} \right) \\ &\quad \left. - \mu_Q k_e (2\mu_Q^2 - m_e^2) - m_e^4 \ln \left(\frac{k_e - \mu_Q}{m_e} \right) \right) \end{aligned} \quad (5.12)$$

where m_n , m_p , and m_e are the rest masses of neutrons, protons, and electrons respectively. By applying (5.8)⁴, we obtain the pressure

$$\begin{aligned} p &= -\epsilon + \sum_{i=n,p,e} \mu_i \rho_i \\ &= \frac{1}{24\pi^2} \left(\mu_B k_n (2\mu_B^2 - 5m_n^2) + 3m_n^4 \ln \left(\frac{k_n + \mu_B}{m_n} \right) \right. \\ &\quad + (\mu_B + \mu_Q) k_p (2(\mu_B + \mu_Q)^2 - 5m_p^2) + 3m_p^4 \ln \left(\frac{k_p + \mu_B + \mu_Q}{m_p} \right) \\ &\quad \left. - \mu_Q k_e (2\mu_Q^2 - 5m_e^2) + 3m_e^4 \ln \left(\frac{k_e - \mu_Q}{m_e} \right) \right) \end{aligned} \quad (5.13)$$

³Note: For brevity, the F denoting the Fermi momentum is omitted from here on. All notations of k_i stand for the corresponding Fermi momentum $k_{F,i}$.

⁴Note that (5.8) is not limited to any choice of chemical potentials. It is thus possible to apply the equation to chemical potentials representing the different particles.

5.2 Charge Neutrality

One finds that any charge of the same sign as the net charge of the star would be expelled by Coulomb force, unless the star's charge is below a certain limit. In [3], it is stated that less than one in 10^{36} baryons is allowed to have an uncompensated charge. For electrons, the number of allowed uncompensated charges is even smaller. We proceed, assuming that the net charge is 0, since 10^{-36} is far beyond the precision of our calculations.

With this argumentation, it would still be possible that charge is differently distributed in the star. Suppose, we had such areas of different charge. In equilibrium the pressure would have to be identical at both sides of the interface between the two phases. Furthermore, the chemical potentials have to be equal at either side. Otherwise, there were more particles moving to the area of lower chemical potential. These two conditions can only be fulfilled, if (i) the areas are alike, or if (ii) we have different phases and thus different EoS in these two areas. Since we excluded phase transitions in our model, the areas have to be alike.

The condition of charge neutrality is given by $\rho_p = \rho_e$. Employing (5.11), we find

$$k_e = k_p \quad (5.14)$$

Applying that k_p and k_e can be expressed analogously to (2.35), we find the relation

$$\mu_Q = \frac{m_p^2 - m_e^2 - \mu_B^2}{2\mu_B} \quad (5.15)$$

5.3 Results

Now, being aware of (5.14) and (5.15), one finds that p and ϵ are functions of only one independent variable μ_B . We are thus allowed to employ (5.10) for our calculations. Before discussing the star's mass, we will analyze the density distribution in a star. The star chosen for figure 3 is the star of maximum mass.

As one sees in figure 3, the star still consists primarily of neutrons. The proton number density and the electron number density⁵, which are demarked by the difference between ρ_B and ρ_n , are small compared to neutron number density. This is also true for other stars of this model. In [3], it is stated that the number density of protons will in no case exceed $\frac{1}{8}$ of the total baryon number density. Hence, we will expect the stars in this section to behave quite like pure neutron stars.

We will now proceed with the $M(R)$ -plot to see what actually happens. In order to compare the results achieved so far, last section's graph was added in figure 4. As we had expected, the maximum mass differs only slightly from the results we obtained for the pure neutron star. Additionally to their small densities, the similar masses of protons and neutrons are also hints to this similar result. The contribution of electrons is negligible, since their masses are very small compared to those of protons and neutrons. With these points in mind, one understands that the results turn out to be similar.

⁵The electron and the proton number density are identical due to the condition of charge neutrality

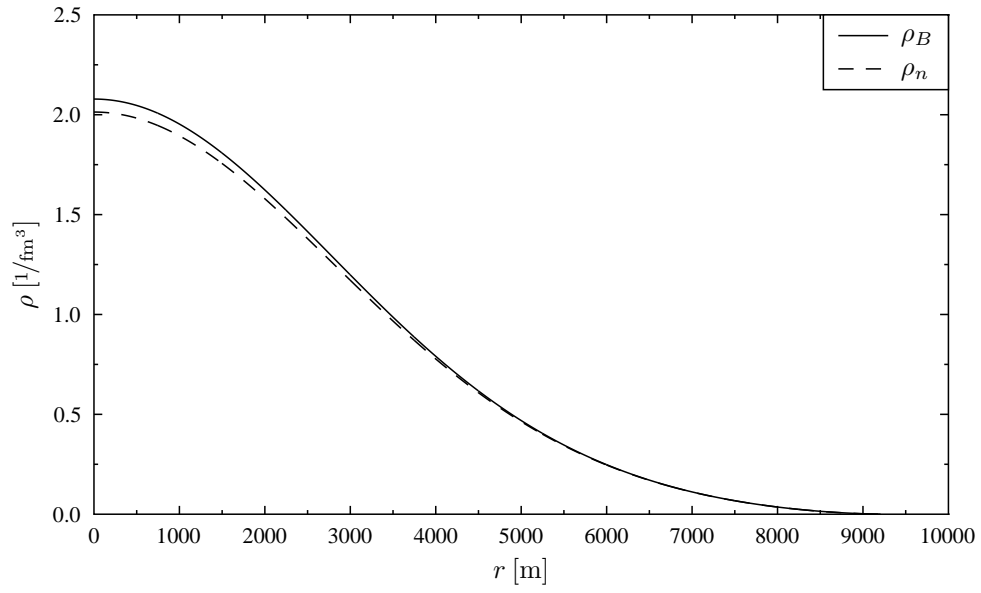


Figure 3: The number density distribution of baryons and neutrons in the star of maximum mass.

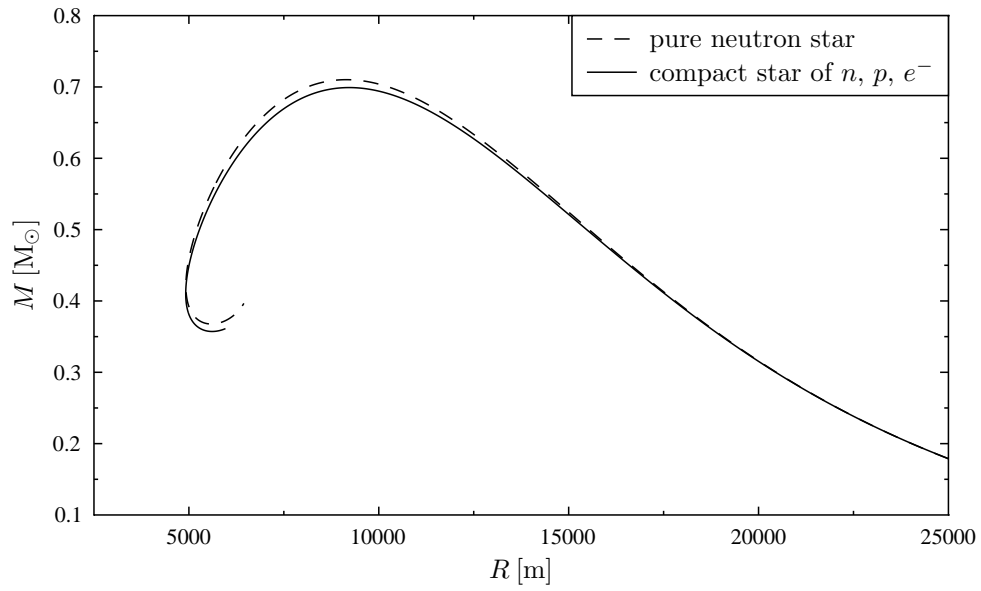


Figure 4: The star's mass M over the star's radius R . The maximum mass is now $0.6991 M_{\odot}$ at 9220 m.

6 Strange Stars

After discussing the two previous equations of state, we are now warmed up to tackle the bag model. In this section we assume that our star consists of up, down, and strange quarks and electrons. Under high pressure (as it can be found inside a compact star) the individuality of nuclei, which are understood as baryons in quantum chromo dynamics (QCD), is lost, leaving 3 quarks [3]. It is thus logical that, instead of an EoS describing hadronic matter, the TOV equation is also integrated for an EoS of quark matter. The bag model which we will use in this section was developed in the 1970ies at the MIT. It was the first model to include color confinement. Color confinement is the effect responsible for keeping three quarks (one of each color) together. In the bag model, this is realized by the bag. Although the three quarks are bound in the bag, they are able to move as they would in case of an ideal Fermi gas within the bag. The size of the bag (which is interpreted as the nucleon size) is represented by the bag constant B . This bag constant is added to the energy density, and represents the energy that is needed to lock the quarks in the bag.

In this section, we will employ the three types of quarks with the lowest masses: up, down, and strange quarks. The magnitude of the chemical potentials in a neutron star is too low for heavier quarks to exist. The chemical potentials of up, down, and strange quarks are given by

$$\begin{aligned}\mu_u &= \frac{1}{3}\mu_B + \frac{2}{3}\mu_Q \\ \mu_s = \mu_d &= \frac{1}{3}\mu_B - \frac{1}{3}\mu_Q\end{aligned}\tag{6.1}$$

where we have again chosen to express the chemical potentials in terms of μ_B and μ_Q . The factor in front of μ_B originates from the fact that, by definition, baryons consist of 3 quarks. Analogously, the factor in front of μ_Q originates from the charge the corresponding quarks carry. As in section 5, we also have $\mu_e = -\mu_Q$. Furthermore, we adapt (2.35) to obtain

$$\mu_f = \sqrt{k_f^2 + m_f^2}, \quad \text{for } f = u, d, s\tag{6.2}$$

Since the quark masses are not listed in [7], the values were taken from [3]

$$m_u = 0.005 \text{ GeV}, \quad m_d = 0.007 \text{ GeV}, \quad m_s = 0.150 \text{ GeV}\tag{6.3}$$

In literature, one finds a wide range of values for the three masses of (6.3). Due to the confinement mentioned above, it is not possible to separate quarks. Consequently, one cannot experimentally measure their mass. Because of this uncertainty, we will vary the strange-quark mass later in this section. One could also do this variation for the other quark masses. We will, however, restrict ourselves to varying m_s , since its magnitude is highest and we may thus expect the greatest changes.

6.1 The Equation of State

The bag model provides us with an EoS that is quite similar to the EoS of degenerate ideal Fermi gases as they were treated in the previous sections. Analogously to

section 5, we derive ρ_f , ϵ_f , and p_f for each kind of quark. Doing so, we have to consider the spin degeneracy, as well as color degeneracy. Color degeneracy leads to an additional factor of 3 [3].

The baryon number density is then given by

$$\rho_f = \begin{cases} \frac{k_f^3}{3\pi^2} & \text{if } \mu_f > m_f \\ 0 & \text{else} \end{cases}, \text{ for } f = u, d, s \quad (6.4)$$

The baryon number density is equal to one third of the corresponding quark number density⁶. In (6.4), we considered the fact that we may encounter a situation, in which the mass of a quark m_f is greater than its chemical potential μ_f computed employing (6.1). In that case, we may say that the chemical potential is not sufficient for this sort of quarks to exist. ρ_f must hence vanish for $\mu_f < m_f$.

As for the energy density and the pressure, we have to bring in the bag-constant B . By definition, B is added to ϵ and subtracted from p .

One discovers that there are some parallels between B and Einstein's famous cosmological constant Λ , when examining the corresponding Einstein field equations $G^{\mu\nu} = kT^{\mu\nu} + \Lambda g^{\mu\nu}$. However, the cosmological constant found experimentally is much lower in magnitude than the range in which we expect to find B .

Continuing with the EoS, we obtain

$$\begin{aligned} \epsilon = B + \sum_{f=u,d,s} \frac{3}{8\pi^2} \left(\mu_f k_f (2\mu_f^2 - m_f^2) - m_f^4 \ln \left(\frac{\mu_f + k_f}{m_f} \right) \right) \\ + \frac{1}{8\pi^2} \left(-\mu_Q k_e (2\mu_Q^2 - m_e^2) - m_e^4 \ln \left(\frac{-\mu_Q + k_e}{m_e} \right) \right) \end{aligned} \quad (6.5)$$

for the energy density and

$$\begin{aligned} p = -B + \sum_{f=u,d,s} \frac{1}{8\pi^2} \left(\mu_f k_f (2\mu_f^2 - 5m_f^2) + 3m_f^4 \ln \left(\frac{\mu_f + k_f}{m_f} \right) \right) \\ + \frac{1}{24\pi^2} \left(-\mu_Q k_e (2\mu_Q^2 - 5m_e^2) + 3m_e^4 \ln \left(\frac{-\mu_Q + k_e}{m_e} \right) \right) \end{aligned} \quad (6.6)$$

for the pressure [3].

Looking at these EoS, we see that if the pressure becomes 0, then the energy density and the baryon number density will not necessarily become 0 continuously. Strange stars have thus "probably [...] the hardest smoothest surface of any object in the universe" [3]. As a consequence we have to take care, when approaching the star's surface in our computation, because the assumption of a locally constant ϵ does not hold for the last step. However, this problem may be solved in a rather simple way. The energy density decreases to 0 at the moment when the pressure becomes 0. In contrast to ϵ , one can still assume that p is linear throughout a step even in this area. Thus, when we encounter $p < 0$ at⁷ $r + \Delta r$, we find that the star's edge is at $r + \frac{p(r)}{-p(r+\Delta r)+p(r)}\Delta r$. Knowing this expression, the correction can easily be included in our program.

⁶The baryon number density is defined this way, because baryons consist of 3 quarks.

⁷ Δr denotes the stepwidth

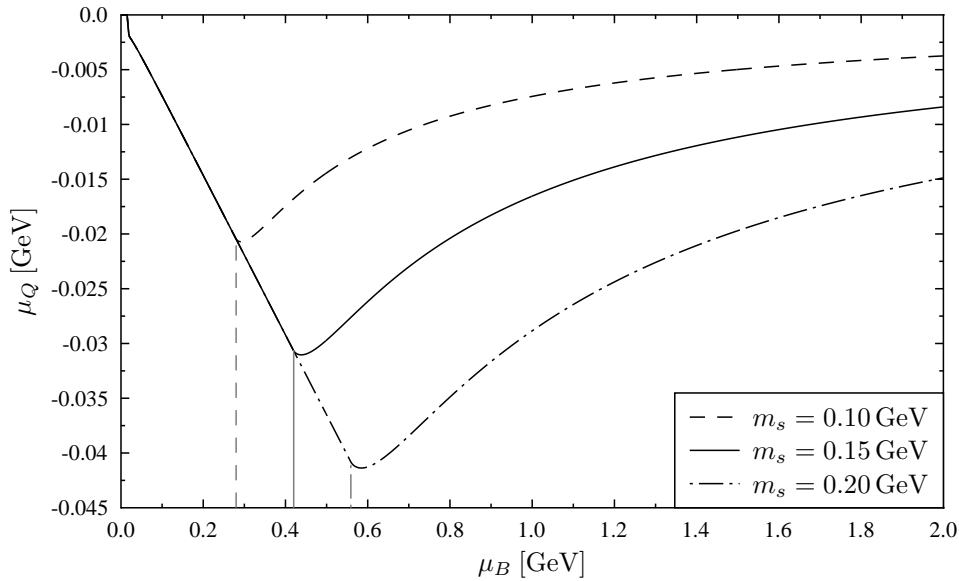


Figure 5: The chemical potential of charge μ_Q as a function of the baryon chemical potential μ_B for different strange quark masses m_s . This function was obtained from the condition of charge neutrality. The vertical grey lines mark the minimum value of μ_B , for which strange quarks can be found for the corresponding strange quark mass.

6.2 Charge Neutrality

As in the previous section, we demand that the star is electrically neutral. However, the resulting condition is more complex in this model, since we have more kinds of particles carrying electrical charge. The condition is now⁸

$$-\rho_e + 2\rho_u - \rho_d - \rho_s = 0 \quad (6.7)$$

which can be rewritten in terms of the Fermi momenta

$$-k_e^3 + 2k_u^3 - k_d^3 - k_s^3 = 0 \quad (6.8)$$

Again, this equation determines μ_Q in terms of μ_B . In contrast to the previous sections, we only find a numerical solution. The result is displayed in figure 5. Note that the sharp bends are observed for $\mu_s = \frac{1}{3}\mu_B - \frac{1}{3}\mu_Q$ which are slightly larger than the corresponding strange quark mass m_s . As discussed in section 6.1, strange quarks are not to be found in regions with $\mu_s < m_s$. For the respective strange quark masses 0.10 GeV; 0.15 GeV; 0.20 GeV, strange quarks can be found if μ_B is greater than 0.28 GeV; 0.42 GeV; 0.56 GeV respectively. Strange quarks have a great influence on the charge potential. Due to their much smaller masses, the respective bends for up and down quarks can be found near $\mu_B = 0$.

⁸Remember that the quark number density is $3\rho_f$

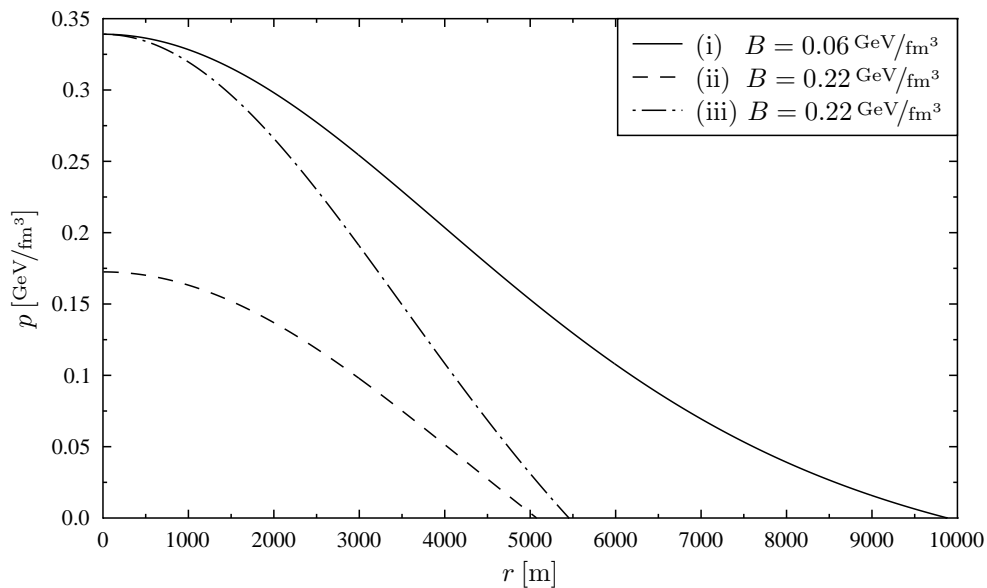


Figure 6: The pressure p versus the distance r from the center. (i) and (ii) depict stars with identical initial values of p_0 (defined in (6.9)) and different values of the bag constant B . (i) and (iii) show stars with identical initial values of p and different values of B .

6.3 Results

For strange stars, we want to discuss the influence of two different parameters, the bag constant B and the strange quark mass m_s .

6.3.1 The Influence of the Bag Constant B

As in the sections before, we begin by analyzing how the stars' structure, i.e. $p(r)$, is changed if B is varied and all other parameters (m_s and the initial baryon chemical potential $\mu_{B,0}$) are kept unchanged. In figure 6, (i) and (ii) are such plots with the same parameters except for B . One observes two aspects of the bag constant's influence on $p(r)$. Firstly, one notices that the main difference between (i) and (ii) is an offset, which is of the size B is varied. Secondly, we find that the gradient of (ii) is slightly smaller than the gradient of (i). At first, we will discuss the effect that p is lowered if B is increased. By formulating pressure and energy density as

$$p = -B + p_0 \quad \text{and} \quad \epsilon = B + \epsilon_0 \quad (6.9)$$

we isolate B in the EoS, and find that p_0 and ϵ_0 are independent of B . Hence, $p_0(r=0)$ and $\epsilon_0(r=0)$ are constant if only B is varied. Since the gradient of $p(r)$ is very similar for (i) and (ii), we find that the initial offset is hardly changed for $r > 0$. This propagation of the offset causes the small radius R of (ii), which is of about half the radius of (i).

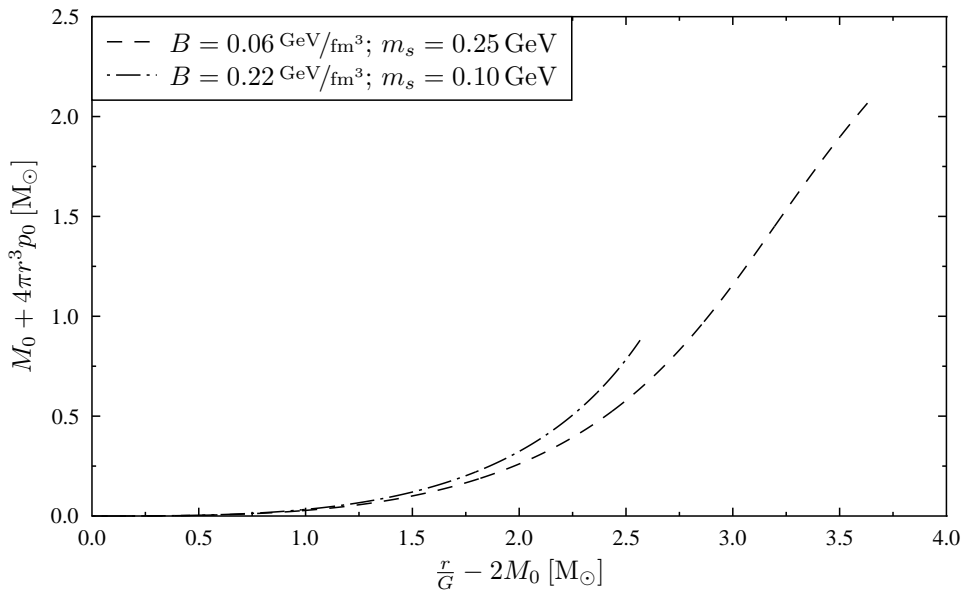


Figure 7: The two terms determining the influence of the bag constant B in a strange star. The x-axis denotes the term of the denominator in (6.11), the y-axis the term of the numerator.

Despite its much smaller significance in determining a star's radius found above, we continue the discussion with the influence of B on the gradient of $\mu_B(r)$. Since $\mu_B(r)$ is closely connected to $p(r)$ by the EoS, the discussion of $\frac{d\mu_B}{dr}$ can be conveyed to the discussion of $\frac{dp}{dr}$ without complications. We will discuss the modified TOV equation here, since it has been used for all calculations of this work. A discussion for the "normal" TOV equation (2.19) would be analogous. As above it is useful to isolate B in the expressions for pressure and energy density. Using (6.9), M then yields

$$M(r) = \frac{4}{3}\pi r^3 B + \int_0^r 4\pi r'^2 \epsilon_0(r') dr' = \frac{4}{3}\pi r^3 B + M_0 \quad (6.10)$$

Deploying (6.9) and (6.10) in our modified TOV equation (5.10), we find

$$\frac{d\mu_B}{dr} = -\frac{\mu_B(M_0 + 4\pi r^3 p_0 - \frac{8}{3}\pi r^3 B)}{r(\frac{r}{G} - 2M_0 - \frac{8}{3}\pi r^3 B)} \quad (6.11)$$

We see that the influence of B on $\frac{d\mu}{dr}$ and thus the star's structure is closely connected to how $M_0 + 4\pi r^3 p_0$ is related to $\frac{r}{G} - 2M_0$. In order to gain an insight into their relationship, both quantities are plotted for two selected strange stars in figure 7. The stars' parameters mark extreme choices of B and m_s . One observes that the denominator is at any point larger than the numerator. Looking at (6.11), we see that $\frac{d\mu}{dr}$ is decreased as B is increased, as we have already noticed in figure 6.

Since the discussion of the two effects is only qualitative, we have to refer to figure 6 to see that the first effect significantly dominates the second one at least in the case

depicted in figure 6. Neglecting the much smaller effect on the gradient, we find that a small change of the bag constant dB (while leaving the initial value of μ_B constant) causes the radius R to decrease by

$$dR = - \left. \frac{dr}{dp} \right|_{r=R} dp = \frac{1}{\left. \frac{dp_0}{dr} \right|_{p_0=B}} dB \quad (6.12)$$

where we have used that due to (6.9) $\frac{dp}{dr} = \frac{dp_0}{dr}$ and $dp|_r = -dB$. The minus sign was introduced, because shifting the whole function $p(r)$ in one direction is equal to shifting the r-axis in the other direction. We may conclude that M also has to decrease for an increased value of B . Using (6.10), (6.12), and $\frac{dM}{dB} = \frac{dM}{dR} \frac{dR}{dB}$, we find

$$\frac{dM}{dB} = 4\pi R^2 (\epsilon_0 + B) \frac{1}{\left. \frac{dp_0}{dr} \right|_{p_0=B}} \quad (6.13)$$

Since the gradient of p is negative, and all other terms on the right hand side of the equation are positive, $\frac{dM}{dB}$ has to be negative. The mass of (ii) must hence be smaller than the mass of (i).

Instead of comparing plots of the same initial baryon potential, one could argue that plots of the same initial pressure had to be compared. In this case, p_0 and thus $\mu_{B,0}$ have to be changed to compensate the variation of B . This situation can be found for (i) and (iii) in figure 6. Again, the surface is reached at a smaller radius for (iii), which can be understood by looking at the modified TOV equation. In (5.10), we find μ_B as a factor at the right side of the equation. $M(r) = \int_0^r 4\pi r'^2 \epsilon(r') dr'$ is also increased if μ_B is. The whole right side of (5.10) is thus likely to be increased in magnitude. As we have seen in figure 6, this increase leads to a larger decrease of (iii) and consequently to a similarly small radius as it was found for (ii).

We expect a similar behavior for a wide range of B and $\mu_{B,0}$, because another value of $\mu_{B,0}$ could only change the discussion at one point. When we compared the two effects of offset and gradient, we referred to the actual choice of $\mu_{B,0}$ employed in the plot. However, since the differences in magnitude between these two effects were found to be very large, a domination of the offset is likely to be found for a wide range of B and $\mu_{B,0}$. When we discussed compensating the offset by increasing $\mu_{B,0}$, we also referred to actual choice of $\mu_{B,0}$. However, since $p(\mu_B)$ is strictly monotonous, this part of the discussion holds true for any choice of $\mu_{B,0}$.

We continue the discussion with the bag constant's influence on the stars' mass limit. As in the section before, we plot the star's masses over the radius. Since we will vary two parameters (B and m_s), we only depict the mass limit⁹ possible for a pair of variates m_s and B in order to avoid confusion. In almost all of the following graphs, we will omit all other points with the same values of m_s and B .

In figure 8, the continuous line is such a curve of maximum masses. There, the maximum masses were obtained for $m_s = 0.15 \text{ GeV}$ and 22 values of B in the range from 50 GeV/fm^3 to 220 GeV/fm^3 . At least for the observed range of m_s and B , the radius of the stars of maximum mass was found to be proportional to the stars' mass, when only the bag constant is varied. A linear least-square-fit returned a slope of

⁹These mass limits were found applying the algorithm described in section 3.4.

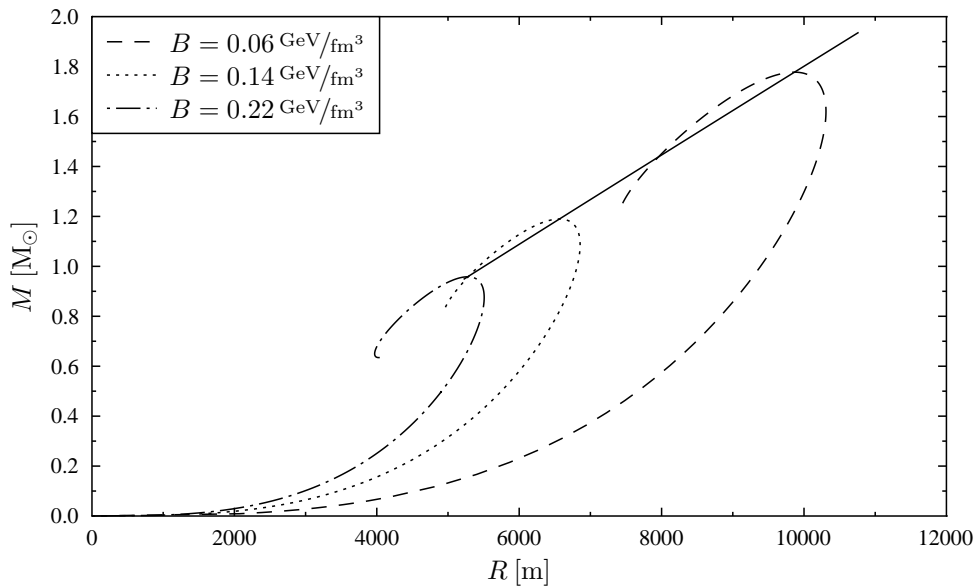


Figure 8: The mass M of strange stars in terms of their radius R displayed for different values of the bag constant B ; the straight line, on which the stars of maximum mass for the strange quark mass $m_s = 0.15$ GeV and $B \in [0.05 \text{ GeV/fm}^3, 0.22 \text{ GeV/fm}^3]$ can be found.

$(181 \pm 0.1)10^{-6} M_\odot/\text{m}$. Similar relations were found for $m_s = 0.10$ GeV; 0.20 GeV; 0.25 GeV.

In figure 9, the mass limit is plotted over the bag constant for different values of m_s . Each of the four curves consists of 22 mass limits found for different combinations of B and m_s . We see that the mass limit is decreased if B is increased. We have observed this behavior in (6.13), when comparing stars of the same initial baryon chemical potential $\mu_{B,0}$. For the stars of maximum mass depicted in figure 9, $\mu_{B,0}$ was found to vary between 1.33 GeV ($B = 0.06 \text{ GeV/fm}^3$) and 1.90 GeV ($B = 0.22 \text{ GeV/fm}^3$) for $m_s = 0.15$ GeV (The ranges for $m_s = 0.10$ GeV; 0.20 GeV; 0.25 GeV were found to be similar). It is hence not possible to adopt the results from the above discussion on the strange star structure. We may yet make some conclusions for strange stars of maximum mass. For the curves in figure 6, the initial values are $\mu_{B,0} = 1.38$ GeV for (i) and (ii) and $\mu_{B,0} = 1.49978$ GeV for (iii). For the stars of maximum mass $\mu_{B,0}$ was determined to 1.3818 GeV ($\simeq 1.38$ GeV) for $B = 0.06 \text{ GeV/fm}^3$ and 1.8853 GeV for $B = 0.22 \text{ GeV/fm}^3$. We see that $\mu_{B,0}$ is even more increased than it would be necessary to conserve the initial pressure for an increased bag constant. The pressure at the center of stars of maximum mass must thus be much higher for a large value of B . Comparing the radii of (iii) and of the star of maximum mass that has also $B = 0.22 \text{ GeV/fm}^3$, we find similar values (5453 m for (iii) and 5265 m for the star of maximum mass). Considering the EoS, we see that the higher value of $\mu_{B,0}$ leads to a much higher mass for the star of maximum mass. By considering how (5.10) changes if $\mu_{B,0}$ is increased, and by looking at figure 9, we find that the steep decrease

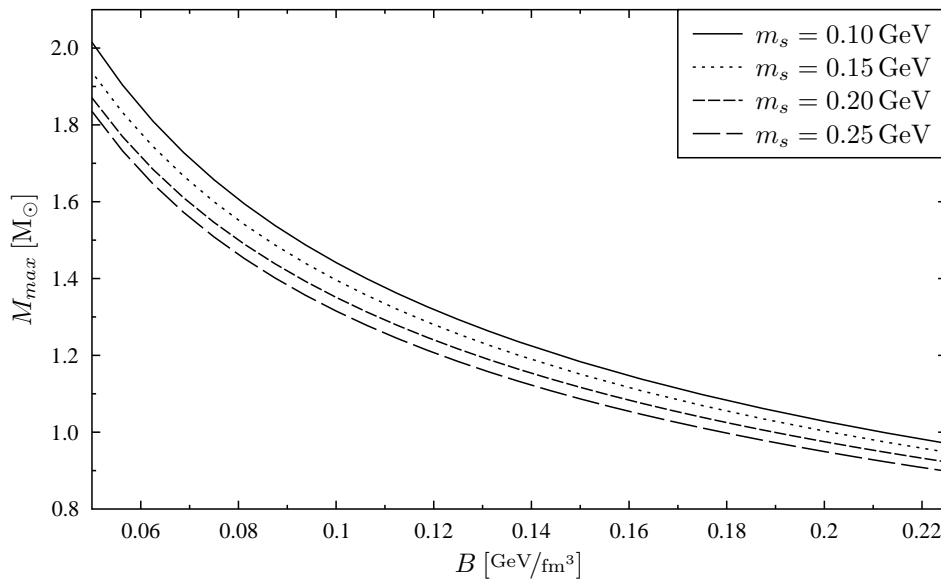


Figure 9: The mass limit M_{max} for strange stars as a function of the bag constant B for different values of the strange quark mass m_s .

of $\mu_B(r)$ and the resulting smaller radius for large $\mu_{B,0}$ lead to a smaller maximum mass, although stars of large $\mu_{B,0}$ have more energy (and thus more mass) stored at the center¹⁰.

Another interesting observation can be made when examining the correlation of the mass limit with the central baryon number density (the sum of all quark baryon number densities). Figure 10 reveals that the settings with high mass limits coincide small central baryon number densities. This behavior is often explained with the stiffness of an EoS. Under the regime of a stiff EoS, strong repulsive forces make it hard to compress matter below a certain density. On the one hand, the strong repulsion in a stiff EoS has to lead to low densities. On the other hand, the stiffer the EoS, the more mass can be included in a star, since the matter withstands more pressure. In the bag model, low values of B lead to stiff EoS, since the pressure is reduced if B is increased.

Comparing the strange star masses computed in this section with the recently reported neutron star mass of $(2.1 \pm 0.2) M_\odot$ which was found for the star PSR J0751+1807 [10], one discovers that extreme choices of B and m_s are necessary to allow a strange star of this mass in the bag model. The existence of such heavy neutron stars suggests that the EoS which describes neutron stars has to be stiffer than the EoS of the bag model. Since the bag model neglects any particle-particle interaction except color confinement, it is not surprising that its stiffness is too low.

¹⁰As a consequence of the EoS, the central energy density is increased if $\mu_{B,0}$ is.

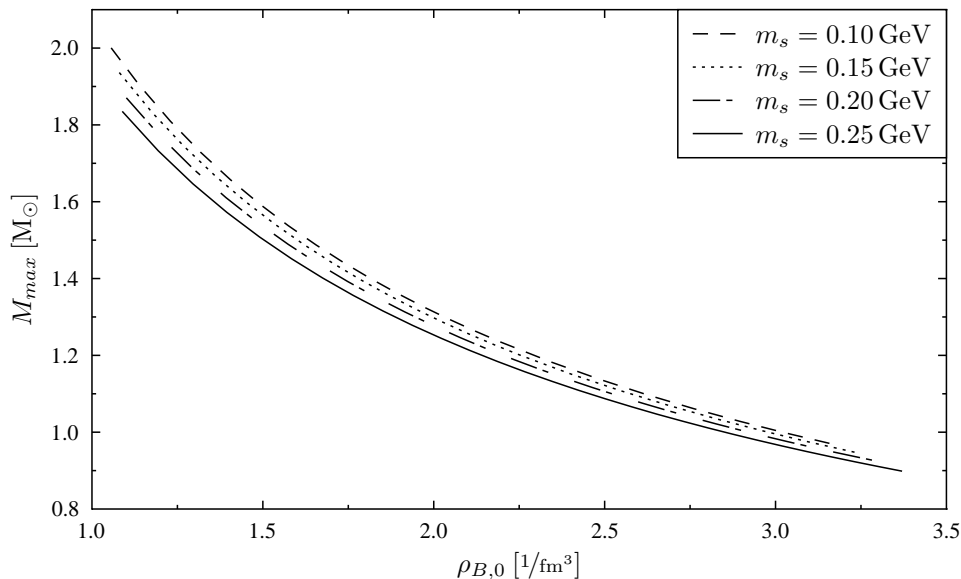


Figure 10: The maximum mass M_{max} of strange stars found for various values of the bag constant B and different values of the strange quark mass m_s versus the central baryon number density $\rho_{B,0}$.

6.3.2 The Influence of the Strange Quark Mass m_s

After studying the influence of the bag constant, we will now focus on the strange quark mass m_s . As mentioned at the beginning of this strange star section, the strange quark mass is not a quantity, that could be determined directly like the mass of e.g. nucleons, due to confinement. The question of how compact stars are affected by the choice of the strange quark mass is thus of great interest and will be discussed in this subsection.

Looking at the EoS, we see that m_s cannot be as easily isolated as it was done for the bag constant in (6.9). In figure 5, we have found that the value of μ_Q (which is required to fulfill the condition of charge neutrality) strongly depends on the value of m_s . As a consequence, the chemical potentials of all particles change if m_s is changed. We find that varying m_s has a significant effect on the density distribution, when looking at figure 11. There, the baryon number densities of up, down, and strange quarks and the number density of electrons are plotted over the strange star radius for $B = 0.14 \text{ GeV}/\text{fm}^3$, $\mu_{B,0} = 1.69 \text{ GeV}$, and different values of m_s . One notices that the strange quark density is decreased for heavier strange quarks. The up quark density is also decreased, although not to the extent the strange quark density is. Since the number of strange quarks is much more reduced than the number of up quarks, this difference has to be compensated by down quarks and electrons due to charge neutrality. One observes that the number density of electrons is at any point at least three orders smaller in magnitude than the quark baryon number densities, and is thus negligible. Due to charge neutrality, one finds that the baryon number

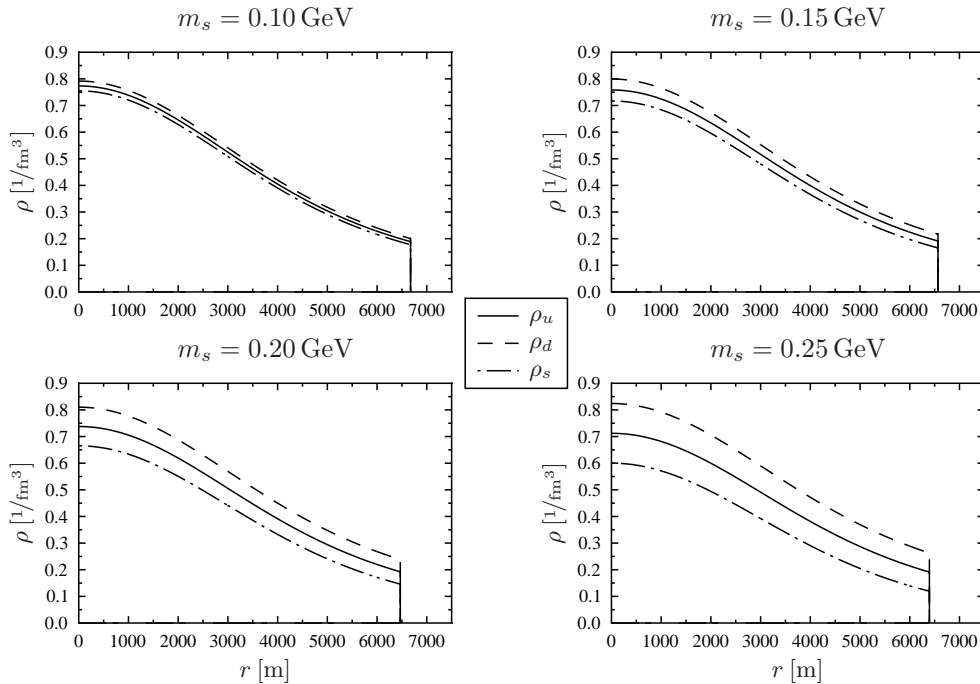


Figure 11: The quark baryon number densities as a function of the distance r from the center with the bag constant $B = 0.14 \text{ GeV}/\text{fm}^3$, the central baryon chemical potential $\mu_{B,0} = 1.69 \text{ GeV}$, and different choices of the strange quark mass m_s .

density of down quarks is increased for heavier strange quarks. An interesting fact which was found when examining the results of the electron number density is that, in contrast to the quark number densities, the electron number density is larger at the surface than at the center of the star.

It was also found that for the four stars displayed in figure 11, $M(r)$ is decreased if m_s is increased. We may thus conclude that the decreased number densities of up and strange quarks outweigh the gain of m_s . As shown in figure 11, the radius becomes also smaller for heavier strange quark masses. Consequently, we expect the total mass to be reduced for heavier strange quarks.

For all stars in figure 11, we chose $\mu_{B,0} = 1.69 \text{ GeV}$. Although this value is close to the values calculated for strange stars of maximum mass with $B = 0.14 \text{ GeV}/\text{fm}^3$ (For stars of maximum mass, $\mu_{B,0}$ ranges from 1.667 GeV for $m_s = 0.1 \text{ GeV}$ to $\mu_{B,0} = 1.748 \text{ GeV}$ for $m_s = 0.25 \text{ GeV}$), we will not make any conclusions from the results of figure 11. Instead, analogous calculations were carried out for respective $\mu_{B,0}$ of stars of maximum mass with different values of m_s . Analyzing the results of these calculations, it was found that only ρ_s is slightly reduced, ρ_u and ρ_d are increased for heavier strange quarks. All other aspects discussed for stars with identical $\mu_{B,0}$ were found to be alike when comparing stars of maximum mass. The energy density was found to be higher for larger m_s .

In figure 12, we observe that the mass limit is decreased if m_s is increased. We may conclude that, although the energy density in the star is higher for heavier strange

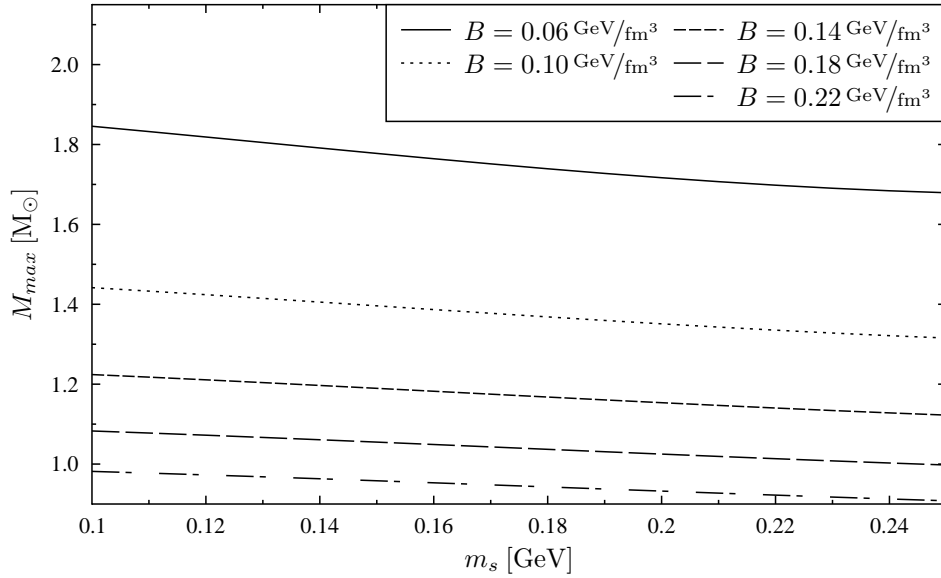


Figure 12: The mass limit M_{max} as a function of the strange quark mass m_s for different values of the bag constant B .

quarks, the reduced radius leads to a smaller mass limit.

Comparing the influences of B and m_s on the strange star mass limit, we find that, within the ranges in which we have varied B and m_s , the influence of the bag constant is much stronger than the influence of m_s . Considering that apart from strange quarks, there are also up and down quarks contributing to the EoS, and that there is the possibility that strange quarks are substituted by down quarks (which have except for the mass the same properties), one finds it not at all surprising that the influence of m_s on the mass limit is much weaker than the one of B .

7 Hybrid Stars

Last section's bag model was introduced in order to describe the quark matter which may be found in regions with high pressure. However, the pressure of a compact star is only near the center high enough to allow deconfinement, if it is at all. Near the surface, the pressure will be comparatively low. Assuming that the ground state of matter is of hadronic nature, we expect quark matter only near the center, while the outer part of a compact star is likely to consist of hadronic matter. In this section, we briefly discuss a few examples of such hybrid stars that combine the bag model with a hadronic EoS taken from [3].

7.1 The Hadronic Phase

The values for the hadronic phase model were taken from the tables 5.10 and 5.7 in [3]. The values of table 5.7 in [3] are in fact due to [11]. The hadronic EoS given there includes nucleons (i.e. neutrons and protons) as well as higher mass baryons (Λ , Σ^+ , Σ^- , Σ^0 , Ξ^- , Ξ^0 , Δ^- , Δ^0 , Δ^+ , and Δ^{++}), which are coupled to σ , ω , ρ mesons. Electrons and muons are also included in the EoS. The EoS obeys the two conditions of baryon number conservation and charge neutrality.

The high density values from table 5.10 cover $\mu_B \in [0.941 \text{ GeV}, 1.54 \text{ GeV}]$ (which corresponds to $\rho_B \in [0.01 \text{ fm}^{-3}, 1.38 \text{ fm}^{-3}]$), while $\mu_B \in [0.930 \text{ GeV}, 0.943 \text{ GeV}]$ (which corresponds to $\rho_B \in [4.73 \cdot 10^{-15} \text{ fm}^{-3}, 8.907 \cdot 10^{-3} \text{ fm}^{-3}]$) is covered by the low density values from table 5.7. During the first calculations of hybrid stars, it turned out that, despite the small range it covers, the low density EoS plays an important role in determining a star's mass and radius, especially if the chosen central baryon chemical potential is low.

Since the tables denote only the baryon number density ρ_B , the energy density ϵ , and the pressure p , the baryon chemical potential μ_B had to be obtained employing $p = \rho_B \mu_B - \epsilon$. For the low density EoS, the calculated values of μ_B were found to scatter. Considering that table 5.7 of [3] denotes only four significant digits for each quantity, one finds by applying error propagation that the deviations can be assumed to be rounding errors. In order to determine an implementable EoS, the set of values had to be approximated by a monotonous function. By substituting a few mavericks by the arithmetic mean of the corresponding two neighboring values, by approximating the first 12 values with $\mu_B = 0.93 \text{ GeV}$, and by finally changing each value to the mean of its neighboring points, a monotonous function was found that is at almost any point within the error bounds of the values from table 5.7. With these modified values, the low density functions $p(\mu_B)$ and $\epsilon(\mu_B)$ were obtained by linear interpolation.

Since the range of μ_B that is covered by the high density EoS is much larger than the range described by the low density EoS, it was possible to interpolate the high density EoS with a spline function, ignoring the numerical deviations of μ_B .

7.2 The Phase Transition

For all phase transitions, we find that two basic conditions have to be fulfilled. At the interface between two phases, the pressure as well as the baryon chemical potential

have to be alike in either phase. If the pressure was not equal at both sides, the resulting net force would lead to an expansion of the phase of higher pressure. If the baryon chemical potential was not continuous at the interface, one would find more particles moving from the phase of higher chemical potential to the phase of lower chemical potential than in the other direction. From thermodynamics, one knows that, in equilibrium, the phase that returns the higher pressure is always favored. By instructing the program to switch the EoS, when the hadronic EoS returns a higher pressure for the current baryon chemical potential, we find the above conditions automatically fulfilled.

In contrast to p and μ_B , ϵ is not expected to be continuous at the interface of our phase transition. Hence, a correction analogous to the one applied at the strange stars' surface (see section 6.1) has been employed at the interface.

There are several ways in which a phase transition could be structured. For instance, there could be an abrupt phase transition or a crossover consisting of homogeneously mixed phases with a continuous concentration gradient. Moreover, it has been proposed that one finds so-called pasta phases consisting of drops, rods, or slabs of one phase immersed in the other (resembling gnocchi, spaghetti, and lasagne) between the pure phases [3]. In a star consisting of two (or more) phases, charge neutrality is not expected to be valid locally, only globally¹¹. Consequently, the components of a mixed phases may have electric net charges. An example for a mixed phase which favors charged components is given in [12]. The presence of strange and down quarks within droplets of quark matter embedded in hadronic matter would decrease the electron chemical potential, permitting a higher proton density in the hadronic phase. As a consequence, the components of the mixed phase carry net charges of opposite sign. However, for our qualitative analysis, we will simplify the calculations by assuming that the phase transition is abrupt.

7.3 Results

At first, we want to briefly examine the influence of a phase transition on the stars' structure, by analyzing an example. Figure 13 presents the pressure and the energy density of a star with a phase transition at $r = 5355$ m. At the interface, we find the expected discontinuity of $\epsilon(r)$ and a bend in $p(r)$. The lower gradient of p in the hadronic phase indicates that the hadronic phase is (at least in the region of the transition) stiffer than the bag model.

Figure 14 demonstrates that the mass and hence the mass limit of hybrid stars strongly depend on the bag constant B . For low central baryon chemical potentials, we find $p(\mu_B)_{\text{hadronic}} > p(\mu_B)_{\text{bag model}}$ at any point inside the star. Although the bag constant determines whether quark matter is included in a star for a certain value of $\mu_{B,0}$, it has no influence on stars without quark matter. The parts of the curves representing pure hadronic stars are thus identical for all three examples displayed in figure 14. At the end of this part, one finds sharp bends in the M - R -graphs and a deviation from the mass of pure hadronic stars for further increased values of μ_B . The occurrence of quark matter obviously reduces the star's mass. This reduction

¹¹Note that, when deriving charge neutrality in section 5.2, we relied on the assumption of having only one phase to find charge neutrality locally valid.

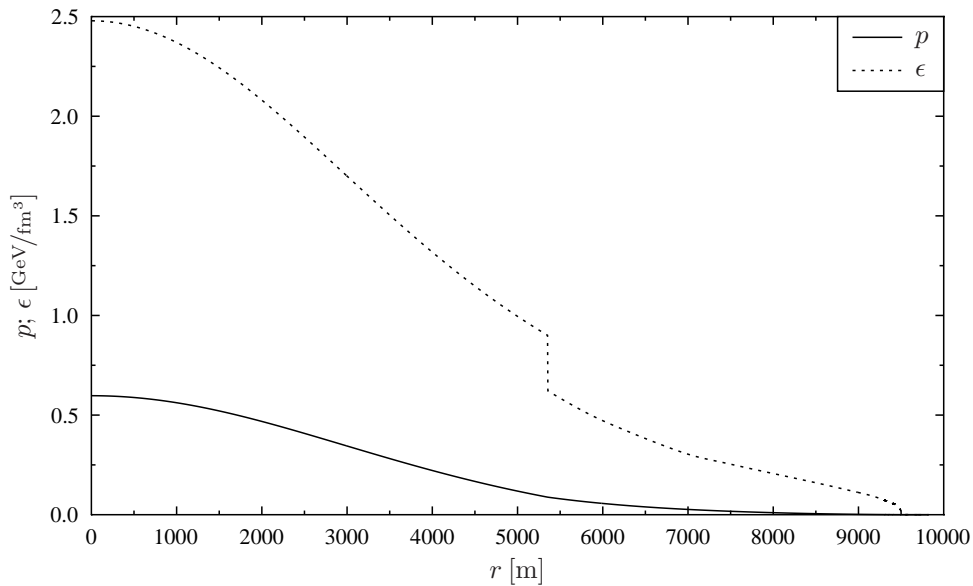


Figure 13: The pressure p and the energy density ϵ versus the distance r from the center for a hybrid star with the central baryon chemical potential $\mu_{B,0} = 1.6 \text{ GeV}$, the strange quark mass $m_s = 0.15 \text{ GeV}$, and the bag constant $B = 0.14 \text{ GeV/fm}^3$.

can be understood as another hint at the lower stiffness of the EoS of the bag model compared to the EoS of the hadronic phase.

For $B = 0.14 \text{ GeV/fm}^3$, we find the maximum mass at the sharp bend of the curve. The star of maximum mass is thus the pure hadronic star with the highest central baryon chemical potential possible for this bag constant. For much higher values of B like $B = 0.22 \text{ GeV/fm}^3$, quark matter plays no physically relevant role. For such values of B , the mass limit of the pure hadronic star is reached without any interference of quark matter. For both values of B mentioned above, all stable stars have to completely consist of hadronic matter. Consequently, if neutron stars were described by hybrid EoS with such values of B , one could not expect to encounter quark matter in neutron stars at all.

For $B = 0.10 \text{ GeV/fm}^3$, we also find a maximum at the bend. Although the curve decreases at first for increasing values of $\mu_{B,0}$, the mass is then found to increase above the level of the first maximum. In contrast to the earlier examples, we observe that there is a significant range of M (including the mass limit) in which one finds hybrid stars including quark matter, as well as hadronic matter.

For low values of B as $B = 0.06 \text{ GeV/fm}^3$, one finds $p(\mu_B)_{\text{hadronic}} < p(\mu_B)_{\text{bag model}}$ for all values of μ_B . This finding contradicts our assumption that the ground state of matter is hadronic, since, with this value of B , there is no point in the EoS where the hadronic phase is stable. However, it has been suggested that there could be "strange quark matter" (SQM) which has a lower energy per baryon than nuclei have [13]. This SQM would thus represent the ground state of matter. Assuming the bag

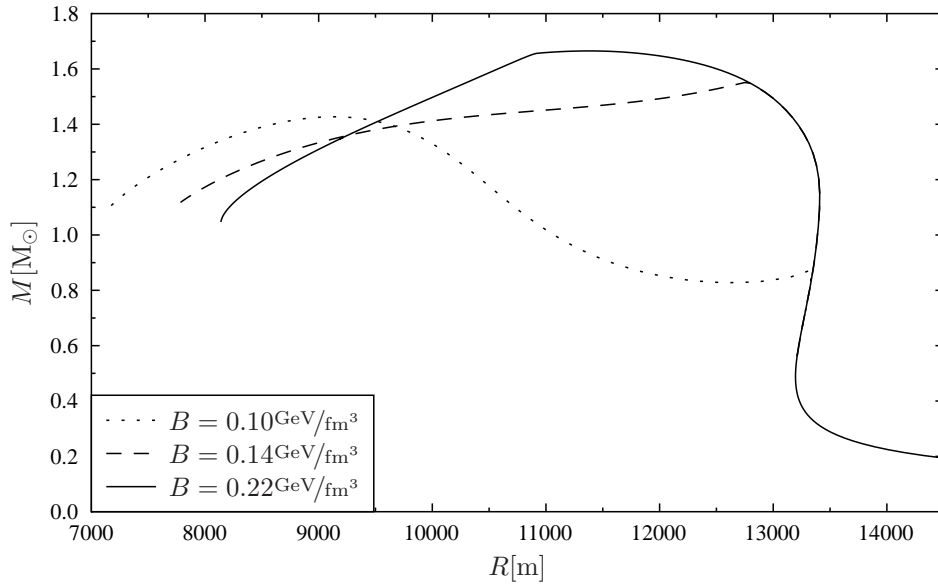


Figure 14: The masses M of hybrid stars against their radii R for the strange quark mass $m_s = 0.15 \text{ GeV}$ and different values of the bag constant B .

model and a strange quark mass of $m_s = 0.15 \text{ GeV}$, it has been found that such strange quark matter could exist for $0.06 \text{ GeV/fm}^3 \lesssim B \lesssim 0.08 \text{ GeV/fm}^3$ [14], which is in good accordance with this example's value of B . Consequently, if SQM really exists, one would find the strange stars discussed in section 6.

Comparing the maximum masses found for hybrid stars with the largest reported neutron star mass of $(2.1 \pm 0.2) M_\odot$ [10], one finds that our EoS is not sufficient to describe real neutron stars. Further improvements of the EoS are thus needed.

8 Summary and Outlook

By integrating the Tolman-Oppenheimer-Volkoff equation, we computed the structure and the mass of compact stars for several given equations of state (EoS) and a set of initial values. In order to obtain a relation connecting the mass and the radius of the stars of an EoS, this computation was repeated for various initial values. In this manner, we were able to determine the mass limit of an EoS which was then analyzed. We started with the rather simple EoS of a pure neutron star and improved it from section to section.

In sections 4 and 5, we have found a maximum mass of about $0.7 M_{\odot}$ for pure neutron stars and for stars consisting of neutrons, protons, and electrons. In section 6, we have found that the properties of strange stars strongly depend on the choice of the bag constant B and the strange quark mass m_s . One observes a reduction of the mass limit, if either B or m_s is increased. For the observed range of B , the maximum mass was found in the range between $0.9 M_{\odot}$ (for $B = 0.22 \text{ GeV}/\text{fm}^3$) and $1.85 M_{\odot}$ (for $B = 0.06 \text{ GeV}/\text{fm}^3$). The relative change of the mass limit was observed to be only about 10% for the variation of the strange quark mass m_s .

Despite its comparatively small influence on the mass limit, the strange quark mass has a strong effect on the constitution of a strange star. It turned out that, due to the condition of charge neutrality, the charge potential μ_Q and hence all involved particle number densities are significantly affected by the choice of m_s . The heavier strange quarks are, the more do the number densities of the different sorts of quarks differ.

A hybrid EoS, i.e. an EoS including quark matter (described by the bag model), as well as hadronic matter, was discussed in section 7. It was found that only for a very limited range of B , one can find stars consisting of both, quark and hadronic matter. For large values of B , the pure hadronic phase prevails.

Further research could analyze the models employed in this work more quantitatively. During this work, it turned out that, for example, the $p(r)$ -curves in figure 6 can be described by functions of the type $p(r) = a \exp(-br^2) + c$. The parameters a , b , and c could be determined to an uncertainty of less than 0.1% when fitting. By finding other, similar functions and probably even functions giving the dependencies of the parameters, it may be possible to track the problem down to an analytic one.

Moreover, it is of great interest to employ other, more sophisticated EoS in the TOV equation. One could, for example, enhance the hybrid EoS of section 7 by (i) substituting the bag model with a model which is better in describing quark matter or by (ii) including more sophisticated phase transitions. (i) could be accomplished by finding EoS that include particle-particle interaction, while (ii) could be accomplished by employing mixed phases like the pasta phases mentioned in section 7.2. One could also improve the hadronic EoS, since not all possible interactions have been included in the employed EoS and since the reported neutron star mass of $2.1 \pm 0.2 M_{\odot}$ cannot be described by a hybrid EoS with this hadronic phase¹².

¹²Here we have assumed that the hadronic phase is stiffer than the quark phase.

References

- [1] R.C. Tolman, Phys. Rev. **55** (1939) 364.
- [2] J.R. Oppenheimer and G. M. Volkoff, Phys. Rev. **55** (1939) 374.
- [3] N.K. Glendenning, *Compact Stars*, Springer, New York, 1996.
- [4] T. Fließbach, *Allgemeine Relativitätstheorie*, Elsevier, Heidelberg, 1998.
- [5] G. Alber, *Vorlesungskriptum Theoretische Physik IV: Statistische Physik*, 2006.
- [6] I.N. Bronstein, K.A. Semendjajew, G. Musiol, *Taschenbuch der Mathematik*, Verlag Harri Deutsch, Thun, 2000.
- [7] GNU Scientific Library (Version 1.7-4), <http://www.gnu.org/software/gsl/>.
- [8] W.-M. Yao et al. (Particle Data Group), J. Phys. **G 33**, (2006) 1.
- [9] M. Buballa, private communication.
- [10] D.J. Nice, E.M. Splaver, I.H. Stairs, O. Löhmer, A. Jessner, M. Kramer, J.M. Cordes, Ap. J. **634** (2005) 1242.
- [11] G. Baym, C.J. Pethick, P. Sutherland, Ap. J. **170** (1971) 299.
- [12] G. Baym, *preprint* nucl-th/0612021.
- [13] E. Witten, Phys. Rev. **D 30** (1984) 272.
- [14] E. Farhi, R.L. Jaffe, Phys. Rev. **D 30** (1984) 2379.

Acknowledgments

I wish to thank Professor Dr. Jochen Wambach for giving me the opportunity of writing this thesis ahead of schedule. I am especially indebted to my supervisor PD Dr. Michael Buballa, with whom I had many helpful discussions and who gave me lots of advice.

I would like to thank my roommate and "sempai" Till Böhlen for many helpful hints on writing with Latex and on programming in C/C++. I also enjoyed the company of my other roommate Sebastian Scheffler, to whom I owe many conversations on physics and on chocolate.

I wish to thank Dominik Nickel, Verena Werth, Markus Hild, Mathias Wagner, and all other members of the NHQ, TNP++, and TPP groups at the Darmstadt Institut für Kernphysik for many stimulating discussions, lots of cake, and the helpful and friendly atmosphere in general.

Finally, I would like to thank my family, my girlfriend Jannike Wolf and my fellow students Anne Sauerwein and Eva Gehrmann for their steady encouragement, their advice, and the - sometimes necessary - distraction. Without their support throughout my studies, this work would not have been possible.